J|A|C|S
ARTICLES

Published on Web 07/06/2009

Structure of a Nickel Chaperone, HypA, from *Helicobacter pylori* Reveals Two Distinct Metal Binding Sites

Wei Xia, Hongyan Li, Kong-Hung Sze, and Hongzhe Sun*

Department of Chemistry and Open Laboratory of Chemical Biology, University of Hong Kong, Pokfulam, Hong Kong, People's Republic of China

Received January 23, 2009; E-mail: hsun@hku.hk

Abstract: Metallochaperones bind metals and ensure the safe delivery of metals to the targets. They are required for the activation and maturation of nickel-containing enzymes [Ni,Fe]-hydrogenase and urease. Metallochaperone HypA was found to be essential to facilitate nickel delivery to hydrogenase together with its partner HypB, although the detailed mechanism is not clear. In this study, we have cloned *hypA* gene from *Helicobacter pylori* (strain 26695), overexpressed, and purified the protein. The zinc-bound HypA (Zn-HypA) exists as a monomer in solution, and its solution structure was determined by NMR spectroscopy together with molecular dynamics simulated annealing. Zn-HypA folds into two domains, including a zinc domain and a nickel domain with a mixed α/β structure. The former houses a rigid zinc-binding site possibly with the role of structural stabilization, whereas the latter harbors a nickel-binding site at the N-terminus. Zinc binds to the four conserved cysteines tetrahedrally as evidenced by ^{113}Cd NMR spectroscopy, and nickel coordinates with four nitrogens of the protein probably in a square-planar geometry. Low coordination number of Ni^{2+} may allow the metal to be readily transferred to its downstream receptors. Our studies may shed light on how the metallochaperone exerts its functions in intracellular nickel delivery.

Introduction

Helicobacter pylori (*H. pylori*) is a peptic ulcer-associated pathogen which is harbored in around 50% of the world's population.[1−3] Two nickel-containing enzymes, urease and [Ni,Fe]-hydrogenase, are crucial for the bacteria's survival and colonization in the mucosa.[4−6] Urease, which accounts for ∼10% of total cellular proteins in *H. pylori* at neutral pH[7] and contains 24 nickel atoms per molecule (dodecamer),[8] catalyzes the hydrolysis of urea into carbamate and ammonia, helping to maintain the bacterial cytoplasm at neutral pH.[9] In addition, [NiFe]-hydrogenase catalyzes the reversible oxidation of molecular hydrogen, providing energy for the bacteria's survival in vivo.[5] Although nickel is an essential element, it is simultaneously toxic when it is in excess. The microorganism must tightly regulate the metal homeostasis through an intricate network of transport from extracellular acquisition to cellular uptake and delivery to end point metallo-enzymes, recycling, and clearance.

In *H. pylori*, nickel is taken up by the nickel-specific permease (NixA)[10] or possibly an ATP-binding cassette-type transport system (ABC transporter).[11] The intracellular nickel is regulated by the nickel-dependent regulator, NikR.[12,13] The histidine-rich proteins, Hpn and Hpn-like, may play a role in nickel storage. These proteins can bind Ni^{2+} moderately and reversibly.[14−17] Interestingly, a heat-shock protein (HspA), a classical GroES chaperonin, has a unique histidine-rich domain in the C-terminus, probably playing a role in nickel binding (or sensing), as well.[18] HspA has been demonstrated to be essential for urease activation by gene complementary experiments.[19] Once the metal enters into the cells, it is likely to be delivered to appropriate apoenzymes, such as urease and hydrogenase, by certain accessory proteins. Genome DNA sequence analysis of

(1) Blaser, M. J. *Gastroenterology* **1987**, *93*, 371–383.
(2) Blaser, M. J. *J. Infect. Dis.* **1990**, *161*, 626–633.
(3) Covacci, A.; Telford, J. L.; Del Giudice, G.; Parsonnet, J.; Rappuoli, R. *Science* **1999**, *284*, 1328–1333.
(4) McGee, D. J.; Mobley, H. L. T. *Curr. Top. Microbiol. Immunol.* **1999**, *241*, 155–180.
(5) Maier, R. J.; Fu, C.; Gilbert, J.; Moshiri, F.; Olson, J.; Plaut, A. G. *FEMS Microbiol. Lett.* **1996**, *141*, 71–76.
(6) Olson, J. W.; Maier, R. J. *Science* **2002**, *298*, 1788–1790.
(7) Bauerfeind, P.; Garner, R.; Dunn, B. E.; Mobley, H. L. T. *Gut* **1997**, *40*, 25–30.
(8) Ha, N. C.; Oh, S. T.; Sung, J. Y.; Cha, K. A.; Lee, M. H.; Oh, B. H. *Nat. Struct. Biol.* **2001**, *8*, 505–509.
(9) Mobley, H. L. T.; Hu, L. T.; Foxall, P. A. *Scand. J. Gastroenterol.* **1991**, *26*, 39–46.
(10) Mobley, H. L. T.; Garner, R. M.; Bauerfeind, P. *Mol. Microbiol.* **1995**, *16*, 97–109.
(11) Hendricks, J. K.; Mobley, H. L. T. *J. Bacteriol.* **1997**, *179*, 5892–5902.
(12) Schreiter, E. R.; Sintchak, M. D.; Guo, Y. Y.; Chivers, P. T.; Sauer, R. T.; Drennan, C. L. *Nat. Struct. Biol.* **2003**, *10*, 794–799.
(13) Dosanjh, N. S.; Michel, S. L. J. *Curr. Opin. Chem. Biol.* **2006**, *10*, 123–130.
(14) Ge, R. G.; Zhang, Y.; Sun, X. S.; Watt, R. M.; He, Q. Y.; Huang, J. D.; Wilcox, D. E.; Sun, H. *J. Am. Chem. Soc.* **2006**, *128*, 11330–11331.
(15) Ge, R. G.; Watt, R. M.; Sun, X. S.; Tanner, J. A.; He, Q. Y.; Huang, J. D.; Sun, H. *Biochem. J.* **2006**, *393*, 285–293.
(16) Zeng, Y. B.; Zhang, D. M.; Li, H. Y.; Sun, H. *J. Biol. Inorg. Chem.* **2008**, *13*, 1121–1131.
(17) Maier, R. J.; Benoit, S. L.; Seshadri, S. *Biometals* **2007**, *20*, 655–664.
(18) Cun, S. J.; Li, H. Y.; Ge, R. G.; Lin, M. C. M.; Sun, H. *J. Biol. Chem.* **2008**, *283*, 15142–15151.
(19) Kansau, I.; Guillain, F.; Thiberge, J. M.; Labigne, A. *Mol. Microbiol.* **1996**, *22*, 1013–1023.

the bacterium[20,21] showed that it has a full set of urease and hydrogenase accessory proteins, which have been well-studied in other bacteria, including urease-related proteins UreIEFGH (encoded by *ure* genes) and hydrogease-related proteins HypABCDEF (encoded by *hyp* genes). The Ni chaperone, UreE, has been proposed to be responsible for the delivery of Ni^{2+} to the UreDFG−urease apoprotein complex in *Klebsiella aerogenes*, probably through the histidine-rich region at the C-terminus.[22]

HypA and HypB proteins form a heterodimer in vitro,[23,24] and high concentration of nickel ions in culture medium was found to partially restore hydrogenase function in *hypA*, *hypB* gene knockout bacteria strains.[25] These studies indicate that these two proteins probably work cooperatively to ensure the nickel delivery to the apo-hydrogenase. It was proposed recently that HypA might serve as a bridging protein between HypB and the hydrogenase large subunit, while HypB, a GTP-binding protein, plays a regulatory role.[24,26] Surprisingly, HypA and HypB also play an important role in the nickel maturation of the urease in most *Helicobacter* species. Disruption of either *hypA* or *hypB* genes resulted in the cessation of hydrogenase activity and 40∼200-fold reduction of urease activity, indicative of a "cross-talk" between the two Ni chaperone systems.[27] The highest urease activity was achieved when HypA was coexpressed with UreE in vivo. Furthermore, a heterodimer complex between *H. pylori* HypA (*Hp*HypA) and UreE was also reported.[28]

Both HypA and its homologue, *Ec*HybF, have been demonstrated to have two different metal binding sites,[24,29] including a high affinity Zn site, possibly playing a structural role, and a relatively low affinity Ni site with the function of donating nickel to its partner proteins. Zn^{2+} was previously proposed to bind four cysteines in the two conserved CXXC motifs in *Escherichia coli* HypA. However, a recent study showed that, in *H. pylori* HypA, Zn^{2+} is coordinated to 3S and 1N/O donor in the absence of Ni^{2+} and changes to 4S coordination upon Ni^{2+} binding,[30] yet the Ni-binding site is less well-characterized.

In this study, we cloned *hypA* gene from *H. pylori* (26695), expressed, and purified the *Hp*HypA, and determined the solution structure of this protein by NMR spectroscopy in combination with molecular dynamics simulated annealing. We characterized the metal-binding properties and validated the two distinct metal-binding sites. Potential functions of the protein were also discussed.

Materials and Methods

Molecular Biology. All chemicals were purchased from Sigma-Aldrich except those indicated. Oligonucleotide primers, plasmids, and bacterial strains used for gene cloning are all summarized in Table S1 (Supporting Information). The genomic DNA was extracted from *H. pylori* 26695 bacteria culture with QIAamp DNA mini kit (Qiagen). The *hypA* gene was then amplified by PCR with designed primers and double digested with *Bam*HI and *Eco*RI restriction endonuclease (New England Biolabs). The digested DNA fragments were purified and subcloned into an expression plasmid with the same digestion sites. The constructed plasmid was sequenced (Invitrogen) to confirm that no mutation occurred during the manipulation.

Expression and Purification of *H. pylori* HypA. *Escherichia coli* BL21 (DE3) (Stratagene), which harbored the expression vector, was grown in 1 L of Luria−Bertani (LB) medium containing 100 μg/mL ampicilin at 37 °C. When the OD at 600 nm reached around 0.6, isopropyl β-D-thiogalactoside (IPTG) was added to a final concentration of 0.2 mM to induce protein expression. Cells were harvested after further incubation for 16 h at 25 °C by centrifugation (4000*g*, 20 min) and then were resuspended in a standard buffer (20 mM Tris-HCl buffer, pH 8.0, containing 300 mM NaCl). Cell pellets were lysed by sonication at 4 °C with 0.5 mM phenylmethanesulfonyl fluoride (Sigma). The supernatant and pellet were separated by centrifugation (10 000*g*, 20 min), and the supernatant was then applied to a HisTrap 5 mL column (Amersham Biosciences) equilibrated with the standard buffer. The column was washed with 25 mL of the standard buffer in the presence of 100 mM imidazole to remove the impurity, followed by washing with 30 mL of the standard buffer. Thrombin (200 NIH units) was then loaded onto the column and incubated at ambient temperature for 8 h. After on-column cleavage, the target protein was eluted with the standard buffer containing 20 mM imidazole. The eluted fraction was pooled, concentrated, further purified by gel filtration using a Hiload 16/60 Superdex 75 column equilibrated with the standard buffer containing 1 mM dithiothreitol (DTT), and concentrated to ∼1 mM. ^{15}N-labeled and ^{15}N/^{13}C-labeled proteins were prepared using M9 medium supplemented with 1 g/L ^{15}N NH_4Cl and 4 g/L ^{13}C glucose (Cambridge Isotope) as sole nitrogen and carbon sources, respectively.

Protein Analysis. Protein concentration was determined by BCA assay kit (Novagen) with bovine serum albumin as a standard. SDS-PAGE was used to examine the purity of final eluted protein (>95%, Figure S1 in Supporting Information). The sequence of the protein was also confirmed by MALDI-TOF analysis.

Inductively Coupled Plasma Mass Spectrometry. ICP-MS was used to determine the metal content of the proteins. Samples for ICP-MS were prepared as reported previously.[15] All experiments were conducted on an Agilent 7500 ICP-MS spectrometer. Each sample was quantified three times, and the average value was used.

UV−Vis Spectroscopy. UV−vis experiments were carried out on a Varian Cary 3E spectrophotometer. An aliquot of Ni^{2+} was added into the Zn-HypA solution in 10 mM HEPES buffer at pH 7.0 containing 50 mM NaCl, in steps of 0.2 molar equiv. Each spectrum of the protein was recorded after equilibrium for 15 min at ambient temperature.

Circular Dichroism (CD). Apo-HypA was prepared as described in Supporting Information. About 20 μM of apo-HypA was prepared in 10 mM HEPES buffer at pH 7.0 containing 50 mM NaCl. CD experiments were carried out at ambient temperature on a JASCO 720 spectrophotometer using a quartz cuvette with a path length of 0.1 or 0.5 cm.

For secondary structure characterization, the CD spectra were recorded from 190 to 260 nm in a step of 0.1 nm at a scan rate of 50 nm/min. Three scans were averaged for each spectrum, and the reference spectrum of the media was subtracted. Protein secondary structure was estimated by CDPro software package.[31]

Urea denaturation experiments were performed as described previously.[32] Different amounts of freshly prepared urea (8 M) were added to both the apo- and Zn-bound HypA in 10 mM HEPES at

(20) Tomb, J. F.; et al. *Nature* **1997**, *388*, 539–547.
(21) Alm, R. A.; et al. *Nature* **1999**, *397*, 176–180.
(22) Song, H. K.; Mulrooney, S. B.; Huber, R.; Hausinger, R. P. *J. Biol. Chem.* **2001**, *276*, 49359–49364.
(23) Mehta, N.; Olson, J. W.; Maier, R. J. *J. Bacteriol.* **2003**, *185*, 726–734.
(24) Atanassova, A.; Zamble, D. B. *J. Bacteriol.* **2005**, *187*, 4689–4697.
(25) Blokesch, M.; Paschos, A.; Theodoratou, E.; Bauer, A.; Hube, M.; Huth, S.; Bock, A. *Biochem. Soc. Trans.* **2002**, *30*, 674–680.
(26) Leach, M. R.; Zamble, D. B. *Curr. Opin. Chem. Biol.* **2007**, *11*, 159–165.
(27) Olson, J. W.; Mehta, N. S.; Maier, R. J. *Mol. Microbiol.* **2001**, *39*, 176–182.
(28) Benoit, S. L.; Mehta, N.; Weinberg, M. V.; Maier, C.; Maier, R. J. *Microbiology* **2007**, *153*, 1474–1482.
(29) Blokesch, M.; Rohrmoser, M.; Rode, S.; Böck, A. *J. Bacteriol.* **2004**, *186*, 2603–2611.
(30) Kennedy, D. C.; Herbst, R. W.; Iwig, J. S.; Chivers, P. T.; Maroney, M. J. *J. Am. Chem. Soc.* **2007**, *129*, 16–17.
(31) Sreerama, N.; Woody, R. W. *Anal. Biochem.* **2000**, *287*, 252–260.

pH 7.0, 50 mM NaCl, to give final concentrations of 10 μM proteins, followed by equilibrium for 12−15 h at ambient temperature prior to data collection. CD spectra were recorded between 220 and 240 nm with an average of three scans using a 0.5 cm cuvette. The ellipticity at 222 nm was used to characterize the unfolding state of the protein.

Visible CD spectrum was collected with 0.25 mM Zn-HypA and nickel-bound Zn-HypA in 10 mM HEPES at pH 7.0 with 50 mM NaCl. A 0.5 cm quartz cuvette was used for spectra record between 300 and 600 nm, with sampling points every 2 nm. Four scans were averaged, and the baseline spectrum of the buffer was subtracted. No smoothing is required for data processing.

NMR Spectroscopy. Triple resonance NMR experiments were performed on a Bruker Avance-600 spectrometer operating at a proton frequency of 600.13 MHz, equipped with a TCI cryoprobe at 298 K. Resonances of Zn-HypA were assigned using spectra acquired with 1−2 mM $^{13}C/^{15}N$-labeled protein in a solution of 20 mM Tris-HCl buffer at pH 7.4, 100 mM NaCl, 95% H_2O/5%D_2O, 0.02% (w/v) NaN_3 and 5 mM tris(2-carboxyethyl)phosphine hydrochloride (TCEP). Backbone and side chain assignments of the protein were accomplished using a combination of $^1H-^{15}N$ HSQC, $^1H-^{13}C$ HSQC, HNCACB, CBCA(CO)NH, HN(CA)CO, HNCO, HBHA(CO)NH, HCCH−TOCSY, and HCCH−COSY spectra. The aromatic side chains were assigned by the analysis of ^{13}C-edited NOESY, $^1H-^{13}C$ HSQC, and 2-D $(H^{\beta})C^{\beta}(C^{\gamma}C^{\delta})H^{\delta}$ and $(H^{\beta})C^{\beta}(C^{\gamma}C^{\delta}C^{\varepsilon})H^{\varepsilon}$ spectra.[33] Interproton distance restraints were derived from three-dimensional ^{13}C-edited NOESY and ^{15}N-edited NOESY spectra with mixing times of 150 ms. ^1H dimension chemical shifts were referenced to 2,2-dimethyl-2-silapentane-5-sulfonic acid (DSS), and ^{13}C and ^{15}N dimensions were referenced indirectly. All NMR data were processed with Bruker XWinNMR software (version 3.5) or NMRPipe[34] and analyzed by Sparky software.[35]

The ^{15}N longitudinal and transverse relaxation time constants, T_1 and T_2, were determined by a series of $^1H-^{15}N$ HSQC spectra using a sensitivity enhanced pulse.[36] For T_1 measurements, the spectra were collected with relaxation delays of 5, 60, 140, 240, 360, 540, 760, and 980 ms. For T_2 measurement, the delays were 16, 32, 48, 64, 96, 112, 128, and 320 ms. Recycle delays (D_1) of 3 and 2 s were used for the T_1 and T_2 measurements, respectively. The T_1 and T_2 values were determined by fitting the cross-peak intensities to a monoexponential function. The steady-state $^1H-^{15}N$ NOE was obtained from a pair of spectra with and without proton saturation. The NOE values were determined as the ratio of the peak volume with proton saturation to that without saturation.

One-dimensional ^{113}Cd NMR spectra were recorded on a Bruker DRX-500 spectrometer at 298 K equipped with a 5 mm BBO probe in the absence or presence of Ni^{2+}. The ^{113}Cd-reconstituted HypA (1 mM) was prepared similarly as described previously.[37] The ^{113}Cd resonance was given in parts per million relative to an external standard $^{113}Cd(ClO_4)_2$ (100 mM).

Two-dimensional $^1H-^{15}N$ HSQC of Zn-HypA was used to monitor the changes of protein backbone (i.e., NH) perturbed by nickel ions. To identify the potential nickel-coordinating histidine side chain(s), 2D $^1H-^{15}N$ heteronuclear multiquantum coherence (HMQC) was performed with a $^2J(^1H,^{15}N)$ of 16 Hz. Upon each stepwise addition of Ni^{2+}, the protein solution stood at room temperature for 15 min prior to NMR spectrum acquisition.

Structure Calculation. Interproton upper bound distance restraints were derived from the NOE cross-peak intensities in 3D $^{13}C-/^{15}N$-edited NOESY spectra at 600 MHz with mixing times of 150 ms. NOE intensities and chemical shifts were extracted by the Sparky software. Torsion angle restraints for φ and ψ angles were obtained from TALOS,[38] and only "good" prediction results were used to create loose restraints with errors of ±60°. Hydrogen bond restraints were derived from hydrogen−deuterium ($^1H-^2D$) exchange experiments as well as NOE patterns. Structure calculations were performed iteratively with CYANA 2.1.[39,40] Structures were calculated without and with the incorporation of Zn−S restraints. The Zn−S bond length was set to 2.3 Å, and the coordination of geometry was constrained to be tetrahedral based on the published data.[41] The standard protocol with seven cycles of structure calculation was applied, and 200 conformers were generated in each cycle with the automated NOE assignments and structure calculation algorithm. In the final cycle, a total of 3288 NOE cross-peaks were assigned from 3512 peaks picked in the NOE spectra, yielding a total of 2001 upper distance limits.

The 30 conformers with the lowest target functions in the final cycle were subjected to further energy-minimization using a generalized Born solvent model[42] using AMBER 7.0.[43] The final 18 energy-minimized conformers were adapted to represent the Zn-HypA structures, and their qualities were evaluated using the PROCHECK.[44] Both the chemical shifts and coordinates of the Zn-HypA were deposited in the BioMagResBank (BMRB: 16126) and the Protein Data Bank (PDBID: 2kdx), respectively. Structures were visualized using MOLMOL[45] and PyMOL.[46]

Results

Characterization of *H. pylori* HypA Protein. The gene encoding HypA was cloned, and the protein was expressed in *E. coli* as an N-terminal GB1-His-tagged recombinant protein and was purified to apparent homogeneity. The purified HypA with Gly−Ser residues remaining at the N-terminal after thrombin cleavage was subjected to gel filtration chromatography and eluted at 74 mL, corresponding to a molecular weight of around 16 kDa (Figure S2 in Supporting Information), consistent with a monomeric form (calcd 13.7 kDa). The bound metal ions in the purified protein were determined by inductively coupled plasma mass spectrometry (ICP-MS) to be less than 0.01 molar equiv of nickel per monomer, whereas it was found to be 0.92 ± 0.06 zinc per monomer, indicative of a fully zinc-bound form of the purified protein.

The CD spectrum (Figure 1A) of purified Zn-HypA in 10 mM HEPES buffer exhibits two negative minima at 208 and 222 nm, indicative of the presence of α-helix secondary structure. The CD spectrum was deconvoluted using CDPro software,[31] which gave rise to 29% α-helix and 24% β-sheet,

(32) Iwig, J. S.; Leitch, S.; Herbst, R. W.; Maroney, M. J.; Chivers, P. T. *J. Am. Chem. Soc.* **2008**, *130*, 7592–7606.
(33) Yamazaki, T.; Formankay, J. D.; Kay, L. E. *J. Am. Chem. Soc.* **1993**, *115*, 11054–11055.
(34) Delaglio, F.; Grzesiek, S.; Vuister, G. W.; Zhu, G.; Pfeifer, J.; Bax, A. *J. Biomol. NMR* **1995**, *6*, 277–293.
(35) Goddard, T. D.; Kneller, D. G. *SPARKY 3*, University of California, San Francisco.
(36) Farrow, N. A.; Muhandiram, R.; Singer, A. U.; Pascal, S. M.; Kay, C. M.; Gish, G.; Shoelson, S. E.; Pawson, T.; Formankay, J. D.; Kay, L. E. *Biochemistry* **1994**, *33*, 5984–6003.
(37) Wang, H.; Zhang, Q.; Cai, B.; Li, H. Y.; Sze, K. H.; Huang, Z. X.; Wu, H. M.; Sun, H. *FEBS Lett.* **2006**, *580*, 795–800.
(38) Cornilescu, G.; Delaglio, F.; Bax, A. *J. Biomol. NMR* **1999**, *13*, 289–302.
(39) Guntert, P. *Prog. Nucl. Magn. Reson. Spectrosc.* **2003**, *43*, 105–125.
(40) Herrmann, T.; Guntert, P.; Wuthrich, K. *J. Mol. Biol.* **2002**, *319*, 209–227.
(41) Hasnain, S. S.; Diakun, G. P.; Abrahams, I.; Ross, I.; Garner, C. D.; Bremner, I.; Vasak, M. *Experientia Suppl.* **1987**, *52*, 227–236.
(42) Tsui, V.; Case, D. A. *Biopolymers* **2000**, *56*, 275–291.
(43) Pearlman, D. A.; Case, D. A.; Caldwell, J. W.; Ross, W. S.; Cheatham, T. E.; Debolt, S.; Ferguson, D.; Seibel, G.; Kollman, P. *Comput. Phys. Commun.* **1995**, *91*, 1–41.
(44) Laskowski, R. A.; Rullmann, J. A. C.; MacArthur, M. W.; Kaptein, R.; Thornton, J. M. *J. Biomol. NMR* **1996**, *8*, 477–486.
(45) Koradi, R.; Billeter, M.; Wuthrich, K. *J. Mol. Graphics* **1996**, *14*, 29–32.
(46) DeLano, W. L. *The PyMOL User's Manual*; DeLano Scientific: Palo Alto, CA, 2002.

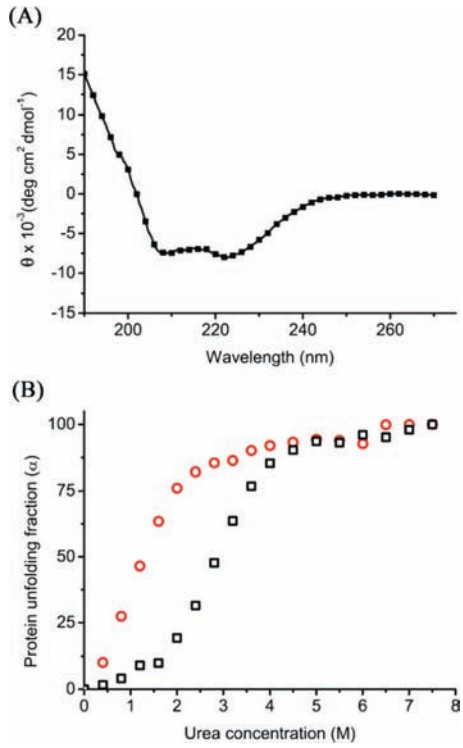

Figure 1. Secondary structure and protein stability of *H. pylori* HypA measured by CD spectroscopy. (A) Far-UV CD spectrum of 5 μM Zn-HypA in 10 mM HEPES at pH 7.0, 50 mM NaCl. Data were converted to molar ellipticity as described.[78] (B) Urea denaturation curve of the apo- (○) and Zn-HypA (□) (10 μM) in the same buffer monitored at 222 nm.

in good agreement with the secondary structure prediction (26% α-helix, 30% β-sheet) obtained by the bioinformatics approach.[47]

Both the apo- and Zn-bound forms of HypA unfolded cooperatively in the presence of high concentration of urea (Figure 1B). The midpoints of denaturation curves of the apo-HypA and Zn-HypA were 1.4 and 3.0 M, respectively, suggesting that Zn^{2+} enhanced the stability of the protein.

Resonance Assignments. Figure 2 shows a 2D $^{1}H-^{15}N$ HSQC spectrum of Zn-HypA in 20 mM Tris-HCl buffer at pH 7.4, 100 mM NaCl. The well-dispersed signals suggest a well-folded protein. HSQC peaks were assigned for all non-proline residues except the N-terminal residues Met1, His2, and Asp60, Ala61, and Leu110. All resonances from side chain NH_2 groups of Asn and Gln residues as well as NH group of Arg residues were identified. Totally, 95.5% of all the ^{1}H chemical shifts were completed for the intact protein. The secondary structure elements consisting of two α-helices and six β-strands were identified by a combination of chemical shift index (CSI) analysis and the pattern of NOEs (Figure S3 in Supporting Information).

Structure Determination and Description. About 3512 manually picked NOE peaks from the 3D ^{15}N-edited NOESY and ^{13}C-edited NOESY spectra with mixing times of 150 ms and 139 TALOS angle and 72 H-bond restraints were used to generate 2001 non-redundant upper limit distance constraints through automated assignment methods. The best 30 structures from CYANA 2.1 were subjected to energy minimization in a force field using the AMBER7 to generate a well-defined

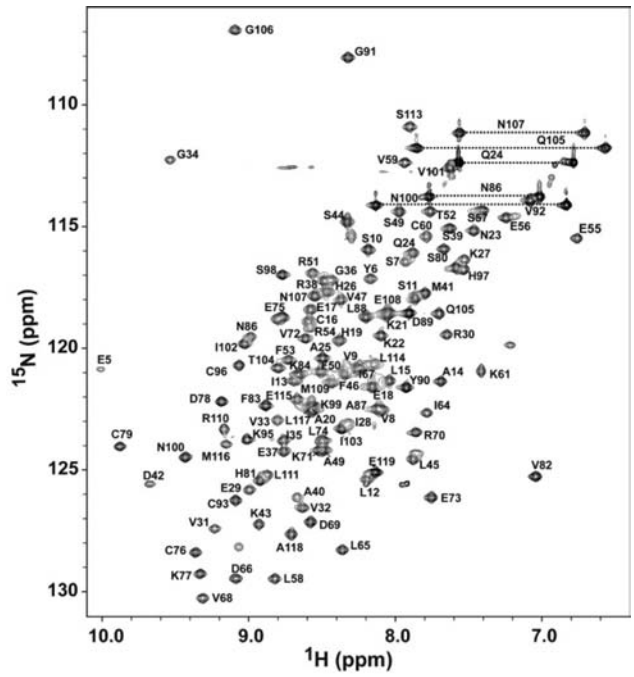

Figure 2. The 600 MHz 2D $^{1}H-^{15}N$ HSQC spectrum of ^{15}N-labeled Zn-HypA in 20 mM Tris-HCl buffer at pH 7.4 with 100 mM NaCl, 5 mM TCEP, 298 K. The assignments are indicated by residue number and one letter amino acid code.

ensemble structure. Statistics for the final 18 structures with the lowest AMBER energies are shown in Table 1. All residues have backbone dihedral angles in allowed regions of ϕ, φ spaces. Procheck analysis yielded an overall G factor of −0.21, indicative of good qualities of the structures.[48] The calculated structures form a tight family with small root-mean-square deviations (rmsd) from the mean structure over well-defined regions (Table 1).

Eighteen lowest energy structures of Zn-HypA were superimposed over the backbone coordinate from residues 2−68, 108−113, and residues 70−104 are shown in Figure 3A,B. Stereoview of a ribbon representation of the lowest energy structure is also shown (Figure 3C). The protein folds into an elongated structure consisting of two domains (nickel domain and zinc domain) with α1-β1-α2-β2-β3-β4-β5-β6 topology. The relative orientation of the two domains is slightly less well-defined, which was also observed in other proteins with two domain structures (e.g., SlyD).[49] The segments that connect to the two domains of HypA comprise Lys69−Val70 and Gly104−Met107. Relatively poor definition between the two domains is likely due to the flexible linker.

The nickel domain consists of 68 N-terminal (residues Met1−Glu68) and 10 C-terminal residues (residues Arg108−Glu117) and contains a Ni-binding site (vide infra). This domain folds into a globular structure, encompassing a three-stranded antiparallel β-sheet flanked on one side by the two α-helices (α1, α2), with a topology of $\alpha\beta\alpha\beta\beta$. Helix 1 and helix 2 are oriented at an angle of around 60° relative to each other. They are stabilized by several hydrophobic interactions which involve residues Val7, Leu10, and Ile11 from helix 1 and Ala47, Phe48,

(47) Rost, B.; Yachdav, G.; Liu, J. F. *Nucleic Acids Res.* **2004**, *32*, W321–W326.

(48) Laskowski, R. A.; Macarthur, M. W.; Moss, D. S.; Thornton, J. M. *J. Appl. Crystallogr.* **1993**, *26*, 283–291.

(49) Weininger, U.; Haupt, C.; Schweimer, K.; Graubner, W.; Kovermann, M.; Bruser, T.; Scholz, C.; Schaarschmidt, P.; Zoldak, G.; Schmid, F. X.; Balbach, J. *J. Mol. Biol.* **2009**, *387*, 295–305.

Table 1. Structural Statistics for the 18 Lowest Energy Structures of Zn-HypA

total number of NOE cross-peaks	3512
non-redundant distance constraints	
total	2001
short range $\|i - j\| = 1$	1142
medium range $1 < \|i - j\| < 5$	323
long range $\|i - j\| \geq 5$	536
H-bond constraints	72
ϕ/ψ dihedral angle constraints (TALOS)	139
residual NOE target function (Å^2)	2.06 ± 0.32
residual NOE distance limit violations	
≥0.40 Å	0
maximum (Å)	0.39
average violation (Å)	0.33 ± 0.05
AMBER energy (kcal/mol)	−4985.95 ± 24.01
rmsd from the mean coordinates (Å)	
residues 1−119	
backbone atoms	1.41 ± 0.32
all heavy atoms	1.92 ± 0.31
residues 2−68, 108−113	
backbone atoms	0.88 ± 0.18
all heavy atoms	1.55 ± 0.15
residues 70−104	
backbone atoms	0.72 ± 0.28
all heavy atoms	1.52 ± 0.32
PROCHECK analysis (all residues)	
residues in most favored region (%)	82.2
residues in additional allowed region (%)	16.9
residues in generously allowed region (%)	0.9
residues in disallowed region (%)	0
overall *G* factor	−0.21 ± 0.03
H-bond energy (kJ/mol)	3.18 ± 0.21
structure *Z* scores (all residues)	
2nd generation packing quality	−2.18
Ramachandar plot appearance	−3.15
$\chi1/\chi2$ rotamer normality	−3.18
backbone conformation	−7.44
rms *Z* scores (all residues)	
bond lengths	0.69
bond angles	1.13
omega angle restraints	1.25
side chain planarity	0.77
improper dihedral distribution	0.75
inside/outside distribution	1.03

and Phe51 from helix 2. A regular hydrogen bond network is formed between the antiparallel sheets. The positioning of the strands is maintained by contacts between hydrophobic residues Ile33, Ile65, Leu63, Leu109, and Leu112 at the β-strands and with residues Phe44, Phe48, Leu10, and Leu13 from the α-helices. This allows a compact packing of the domain.

The zinc domain is formed by 33 residues (Glu71−Gln103) containing two pairs of conserved CXXC motifs, which is a typical Zn-binding motif.[50] This domain is dominated by a three-stranded antiparallel β-sheet and a bulge loop (loop 6 with residues of Lys82−Val99). The Zn^{2+}-binding site is located at this domain, which spans residues Cys74−Cys94. The binding site is formed by loop 5 (Cys74−His79), which provides Cys74 and Cys77, and the loop 6 (Lys82−Val99), which provides Cys91 and Cys94. To exclude bias associated with forcing a certain Zn^{2+} coordination scheme, the structures of Zn-HypA were also calculated without Zn−S constraints, which showed that the side chains of the putative coordinating residues (Cys74, Cys77, Cys91, and Cys94) are positioned suitably to allow Zn^{2+} coordination (Figure S4 in Supporting Information). The presence of a histidine at position 95 (His95), which is next to zinc ligand Cys94, may cause ambiguity in the zinc coordination.

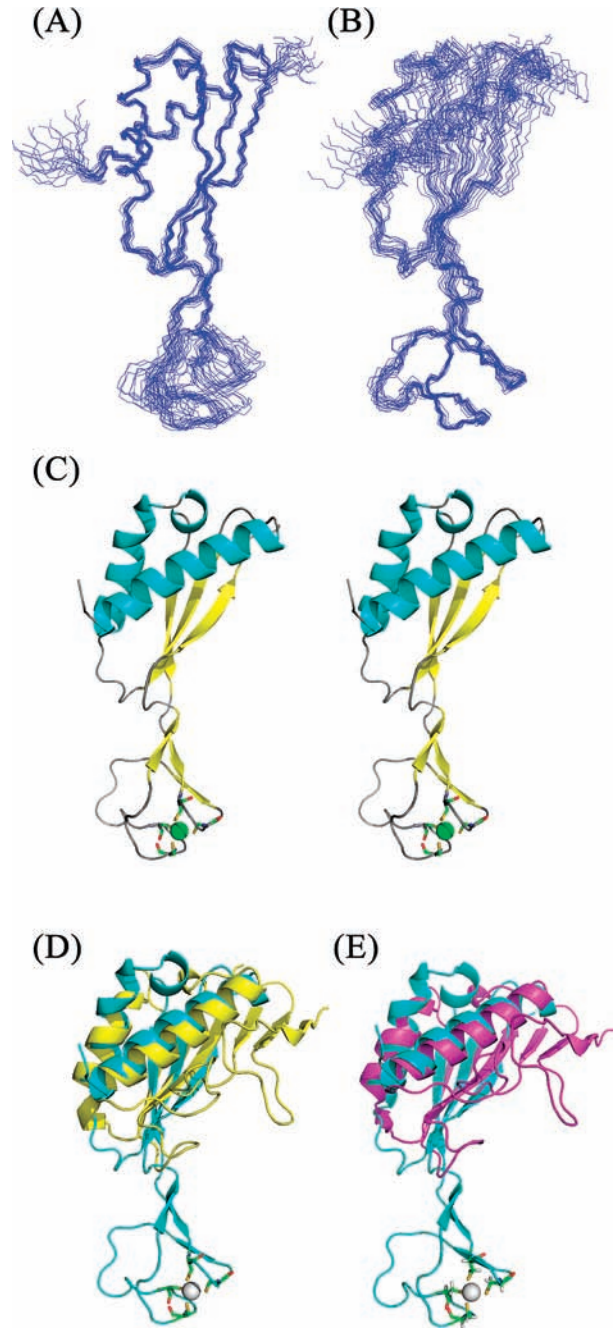

Figure 3. Solution structures of *Hp*HypA. The 18 structures of the lowest-energy Zn-HypA are superimposed for the nickel-binding domain (residues 2−68, 108−113) (A) and zinc-binding domain (residues 70−104) (B). Stereoview of the lowest energy structure after energy minimization. (C) Rigid secondary structures of the protein are assigned with different colors. The lowest energy structure of Zn-HypA (cyan) superimposed on the homologue structures (D) PDB: 1X25-B (yellow); (E) PDB: 2ewc-B (purple).

Such ambiguity was excluded by both the peak pattern and the chemical shift of histidine ring nitrogens determined from a 2D $^1H-^{15}N$ HMQC spectrum, which did not support a Zn-His95 coordination (vide infra).

Structural Comparison of HypA with Other Proteins. Protein structure homologue searches were carried out using DALI server.[51] The results gave rise to 47 proteins with the *Z* score

(50) Berg, J. M. *J. Biol. Chem.* **1990**, *265*, 6513–6516.

(51) Holm, L.; Sander, C. *Trends Biochem. Sci.* **1995**, *20*, 478–480.

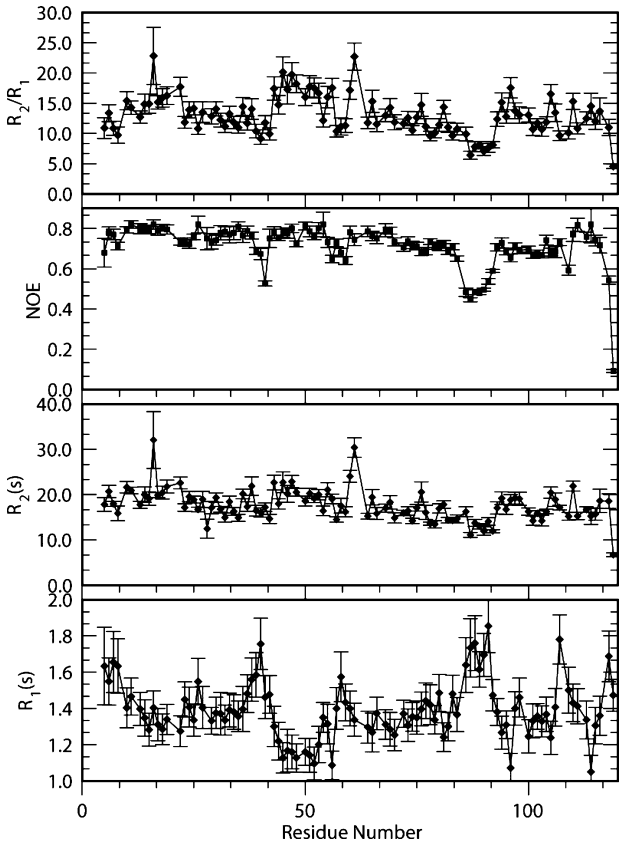

Figure 4. ^{15}N relaxation data and ^{15}N−^{1}H heteronuclear NOE for Zn-HypA. The values of R_1, R_2 NOE for each residue are shown as a function of residue number in the protein sequence.

over 4.0, most of which are in different functional protein families. However, none of these proteins has a close resemblance to the HypA structure with a rmsd value less than 2.0. The best two results are two hypothetical proteins: PDB number 1X25 (chain B) with a *Z* score of 7.1, rmsd of 2.7, and 2ewc (chain B) with a *Z* score of 6.7, rmsd of 2.6. With the aid of DaliLite, the HypA structure was aligned with these two structures (Figure 3D,E). Notably, no similar fold of the zinc domain has been found in the atomic coordinates deposited in the PDB database, indicative of a unique structure of this domain.

Protein Backbone Dynamics. The backbone dynamics of Zn-HypA were assessed by measuring the ^{15}N relaxation parameters, R_1 ($1/T_1$), R_2 ($1/T_2$), and the steady-state heteronuclear NOEs, and the results are shown in Figure 4. Out of 114 assigned residues, 100 were used for the analysis and 14 were excluded due to spectral overlap. On the basis of the ^{1}H−^{15}N NOE data, the backbone of Zn-HypA is relatively rigid on the picosecond−nanosecond scale. Increase in mobility was noted in the loop 2, loop 6, and the C-terminus. Interestingly, although loop 6 is extended from residues Lys82−Val99, only a portion (Asn84−Val90) of it exhibits high mobility, possibly due to zinc coordination at Cys91 and Cys94, which have restrained the movement of the loop. The R_1 and R_2 generally are in agreement with NOE data. The average overall rational time (τ_c) was estimated from the 10% trimmed mean values of R_2/R_1 for the backbone amide ^{15}N to be 11.2 ns.

Zinc Coordination. A close inspection of the sequence alignment reveals the presence of four completely conserved cysteine residues, Cys74, Cys77, Cys91, and Cys94 in two CXXC motifs (Figure 5). His95 is also a putative zinc-binding residue, although it is not conserved. The complete assignments for the six cysteines show that the chemical shifts of the β-carbons (C^{β}) of C16 and C60 are 26.9 and 28.2 ppm, respectively, for the Zn-HypA. In contrast, the chemical shifts of the β-carbons of C74, C77, C91, and C94 are downfield shifted by over 4 ppm (between 31.1 and 32.5 ppm). Such downfield shifts have commonly been observed in many zinc-finger proteins and used as an indicator for zinc coordination with thiolate sulfurs of cysteine residues.[52] Long-range 2D ^{1}H,^{15}N heteronuclear multiple quantum coherence (HMQC) was acquired to distinguish different tautomeric forms of histidine imidazole rings. The observed pattern and chemical shifts of nitrogens for the uniformly ^{15}N-labeled Zn-HypA indicate that His95 does not involve in zinc binding.

^{113}Cd NMR has been widely used to probe zinc binding in metalloproteins.[53] To further confirm the zinc coordination sphere, ^{113}Cd-reconstituted HypA was prepared, and one-dimensional ^{113}Cd NMR of the protein under identical conditions to the Zn-bound form yielded only one peak at 736 nm (Figure S5 in Supporting Information), which is characteristic for Cd^{2+} binding to four thiolates tetrahedrally,[54] indicating that Zn^{2+} is coordinating to four cysteines. It should be noted that neither the line width nor the chemical shift of ^{113}Cd resonance changed upon the addition of 1.0 molar equiv of Ni^{2+} (Figure S5 in Supporting Information), indicating that nickel binding does not perturb zinc coordination.

Nickel Coordination. Nickel binding to Zn-HypA protein was first monitored by UV−vis spectroscopy. As shown in Figure 6A, two major absorption bands increased with the addition of nickel ions. One intense band at 250 nm could be assigned to N → Ni(II) LMCT transition ($\varepsilon = 3250\ M^{-1}\ cm^{-1}$), whereas a relatively weak band at ca. 420 nm ($\varepsilon = 96\ M^{-1}\ cm^{-1}$) with a shoulder at 494 nm linearly increased up to 1 equiv of Ni^{2+} (Figure S6 in Supporting Information), which could be assigned to a d−d transition of nickel,[55] similar to other nickel-binding proteins.[15,56] It is characteristic for a planar coordination of Ni^{2+} in a 4N chromophore.[57] Subsequently, CD spectroscopy was used to further investigate nickel coordination, and no absorption was observed at a visible region (300−600 nm) for Zn-HypA. Upon addition of Ni^{2+}, a positive peak at 410 nm and negative peak at 480 nm were clearly observed (Figure 6B). Such peaks are again characteristic for Ni^{2+} coordination with 4N in peptides and proteins.[58]

Two-dimensional ^{1}H−^{15}N HSQC was also used to investigate Ni^{2+} binding to the protein with the aid of ^{15}N-labeled Zn-HypA. Upon the addition of 0.8 molar equiv of Ni^{2+}, the cross-peaks of two residues, Glu3 and Asp40, disappeared (Figure 7A). However, no observable line broadening was detected for the cross-peaks of those residues sequentially close to these two residues, such as Tyr6, Met39, and Lys41 (data not shown), indicating that the bound nickel is diamagnetic. Disappearance of the cross-peaks of Glu3 and Asp40 is therefore not attributed

(52) Moller, H. M.; Martinez-Yamout, M. A.; Dyson, H. J.; Wright, P. E. *J. Mol. Biol.* **2005**, *351*, 718–730.
(53) Vašák, M. *Biodegradation* **1998**, *9*, 501–512.
(54) Coleman, J. E. *Methods Enzymol.* **1993**, *227*, 16–43.
(55) Lever, A. B. P. *Inorganic Electronic Spectroscopy*, 2nd ed.; Elsevier: Amsterdam, 1984.
(56) Chivers, P. T.; Sauer, R. T. *J. Biol. Chem.* **2000**, *275*, 19735–19741.
(57) Zoroddu, M. A.; Schinocca, L.; Kowalik-Jankowska, T.; Kozlowski, H.; Salnikow, K.; Costa, M. *Environ. Health Perspect.* **2002**, *110*, 719–723.
(58) Sigel, H.; Martin, R. B. *Chem. Rev.* **1982**, *82*, 385–426.

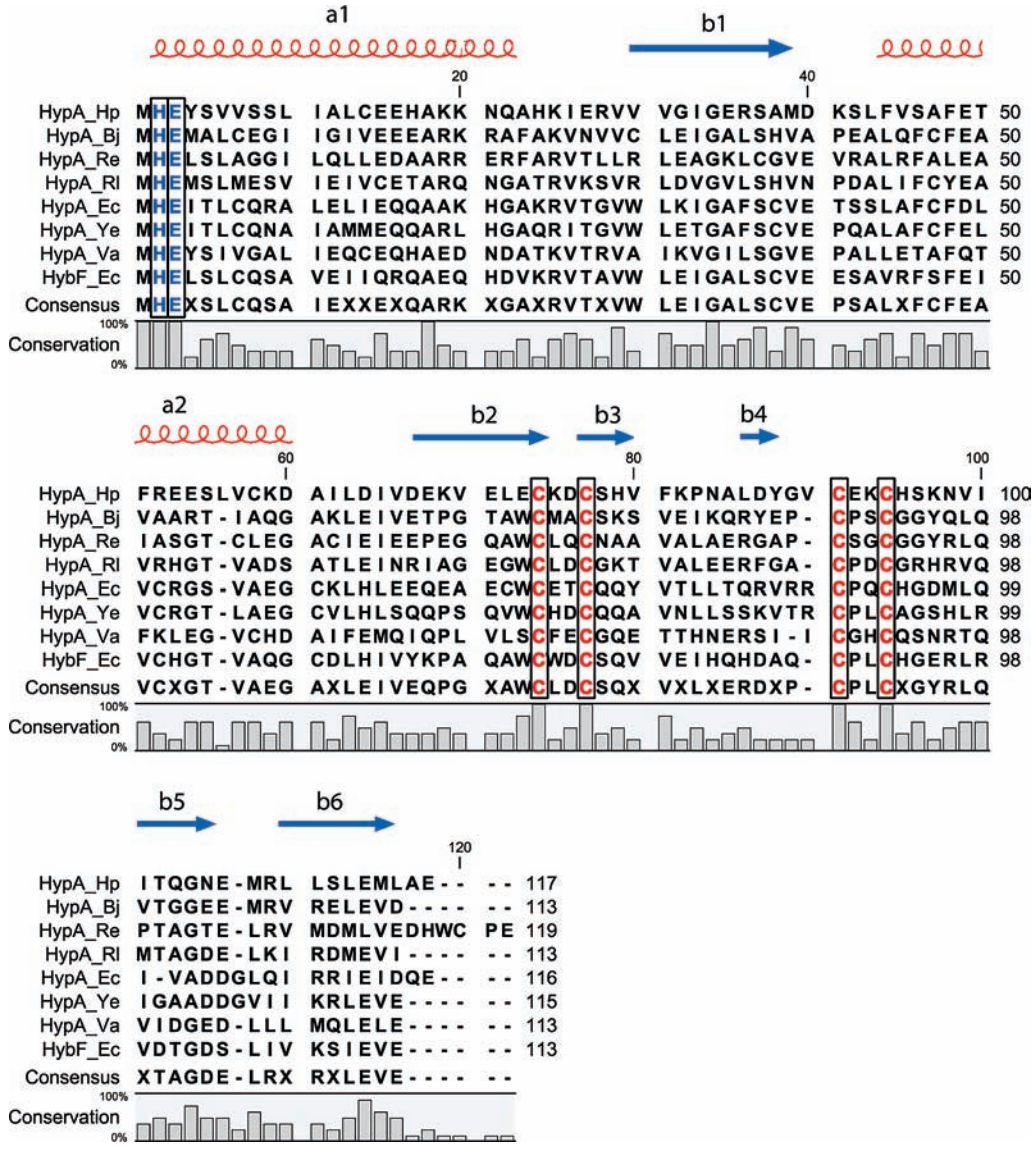

Figure 5. Sequence alignment of HypA proteins. The secondary structure elements are shown on top of the figure. The conserved His2, Glu3, and the two CXXC motifs are highlighted. Schematic drawing of the conservation for each residue is included. UniprotKB accession numbers are *Helicobacter pylori* HypA, Q7 VI03; *Bradyrhizobium japonicum* HypA, Q45256; *Ralstonia eutropha* HypA, P31901; *Rhizobium leguminosarum*, P28154; *Escherchia coli* HypA, A8A3K4; *Yersinia enterocolitica* HypA, A1JTY8; *Vibrio angustum* HypA, Q1ZT06; *Escherchia coli* HybF, A1AFQ5.

to the line broadening induced by nickel; instead, it might be caused by the deprotonation of amides of the backbone of Glu3 and Asp40, due to nickel coordinated to the backbone nitrogens, which is a common feature for many nickel-binding peptides or proteins with a square-planar geometry.[59−61]

Unexpectedly, a new set of peaks appeared for certain residues upon Ni^{2+} binding (data not shown). With the increase in nickel concentration, the intensities of original peaks decreased while those of new peaks increased in intensities (e.g., Ala38, Leu56, and Val66), indicating that the nickel-free and nickel-bound forms of the protein were in a slow exchange on the NMR time scale.[62] The changes of chemical shifts were subsequently mapped onto the three-dimensional structure of Zn-HypA (Figure 8). The regions perturbed by nickel mainly clustered at the N-terminal region, a part of the β-strand regions (Leu63−Asp67, Arg108−Ala116) and the turn where the residue Asp40 is located (e.g., Glu35, Ala38, and Glu71).

To investigate whether histidine side chains are involved in Ni^{2+} binding, 2D $^{1}H-^{15}N$ HMQC spectra optimized for two- and three-bond couplings between the ring N atoms and nonexchangeable ring protons of histidine residues were recorded for the Zn-HypA and Ni^{2+}-bound form of the protein. In combination with 2D $^{1}H-^{13}C$ HSQC, 2D $(H^{\beta})C^{\beta}(C^{\gamma}C^{\delta})H^{\delta}$, and ^{13}C-edited NOESY, complete assignments for the side chains of all five histidine residues were achieved for the protein. The 2D HMQC spectra with assignments of Zn-HypA are shown in Figure 9A. On the basis of the observed pattern and chemical shifts of the peaks, His2, His17, H24, and His79 were found to be in the neutral tautomeric forms with $N^{\varepsilon 2}$ protonated,

(59) Jones, C. E.; Klewpatinond, M.; Abdelraheim, S. R.; Brown, D. R.; Viles, J. H. *J. Mol. Biol.* **2005**, *346*, 1393–1407.
(60) Van Horn, J. D.; Bulaj, G.; Goldenberg, D. P.; Burrows, C. J. *J. Biol. Inorg. Chem.* **2003**, *8*, 601–610.
(61) Wuerges, J.; Lee, J. W.; Yim, Y. I.; Yim, H. S.; Kang, S. O.; Carugo, K. D. *Proc. Natl. Acad. Sci. U.S.A.* **2004**, *101*, 8569–8574.
(62) Wüthrich, K. *NMR of Proteins and Nucleic Acids*; Wiley: New York, 1986.

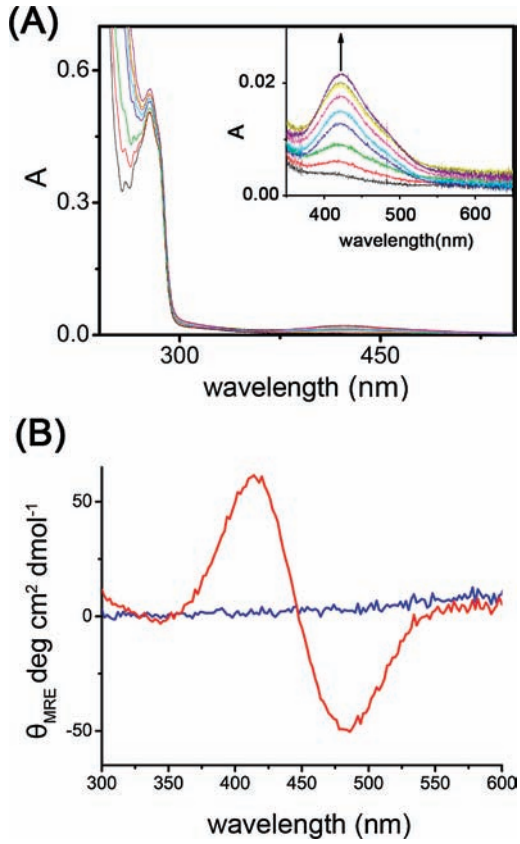

Figure 6. UV−vis and CD spectra of HypA. (A) UV−vis spectra of HypA (0.2 mM) upon addition of Ni^{2+}. The spectra were recorded with Zn-HypA with stepwise addition of Ni^{2+}. The inset shows a typical weak d−d transition band at 420 nm and a shoulder at around 490 nm. (B) CD spectrum of 0.25 mM Zn-HypA (blue) and nickel-bound Zn-HypA protein (red). The two diachronic bands at 480 and 410 nm are characteristic for a square-planar geometry of the Ni(II)N_4.

while His95 was protonated on both $N^{\delta 1}$ and $N^{\varepsilon 2}$.[63] Upon addition of nickel, significant downfield shifts were observed for His2 signals, particularly in the ^{15}N dimension; that is, $N^{\delta 1}$ shifted by 17.7 ppm (from 220.5 to 238.2 ppm), whereas $H^{\varepsilon 1}$ shifted slightly from 7.82 to 7.87 ppm without observable broadening (Figure 9B). This is again a strong support of a diamagnetic bound nickel. In contrast, the chemical shifts of both $N^{\delta 1}/N^{\varepsilon 2}$ and $H^{\varepsilon 1}/H^{\delta 2}$ of other four histidine residues remained almost unchanged. Such an evident downfield shift of $N^{\delta 1}$ of His2 is attributed to Ni^{2+} coordinating to this atom. Similar phenomenon has commonly been observed in certain zinc-finger proteins upon zinc binding.[52] It was also noticed that slight changes occurred for $H^{\varepsilon 1}$ of His95 but not for $N^{\delta 1}$ or $N^{\varepsilon 2}$, which is likely due to the conformation change upon nickel binding, in agreement with the observation that nickel binding is accompanied by structural changes.

Discussion

Metallochaperones are a family of soluble metal-binding proteins acting in the intracellular metal ions trafficking.[64] Enormous efforts have been made to understand the pathways of copper trafficking within mammalian cells and yeasts in the past decade. For example, three distinct copper trafficking pathways have been identified and extensively characterized. Each of the specific chaperones, such as Atx1, delivers Cu^+ to the active site of its target enzyme through a "hand-shake" mechanism.[65−67] The Ni chaperone, UreE, is responsible for the delivery of nickel ions into the urease active site.

HypA is a nickel chaperone for maturation and activation of hydrogenase. In *H. pylori*, the protein was also found to be important for urease maturation. HypA was proposed to interact with its partner, HypB, which is a small GTPase to deliver nickel

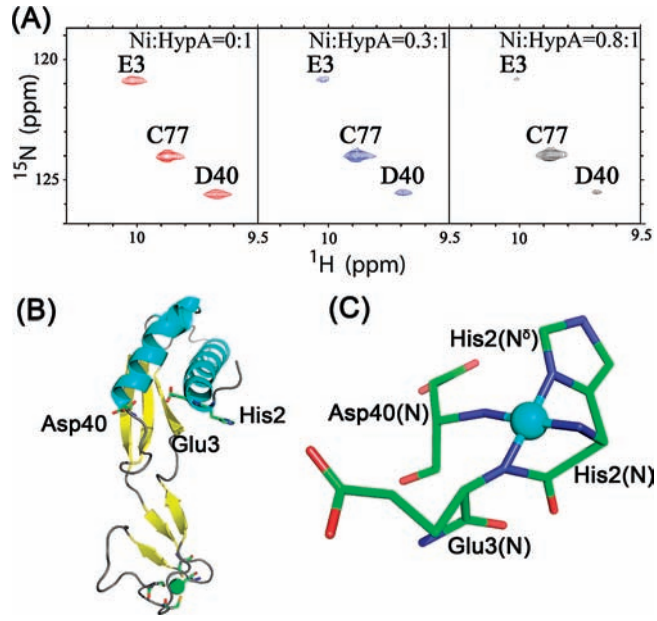

Figure 7. Characterization of Ni-binding site of HypA. (A) Two-dimensional $^1H-^{15}N$ HSQC spectra after addition of different molar ratios of Ni^{2+} reveal a diamagnetic Ni. The cross-peaks of Glu3 and Asp40 disappear upon addition of Ni^{2+}. (B) Structure of HpHypA with putative nickel-binding residues His2, Glu3, and Asp40 highlighted. (C) Proposed square-planar Ni site with four binding ligands, His2 (N), His2 (N^{δ}), Glu3 (N), and Asp40 (N).

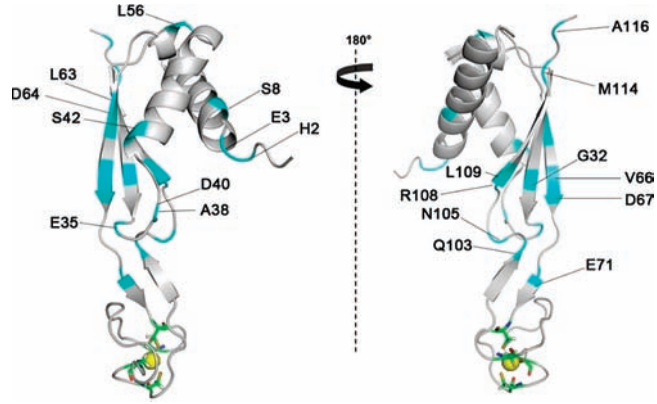

Figure 8. HypA structures showing the location of residues (in cyan) perturbed upon Ni^{2+} binding based on nickel titration experiments, indicating conformational changes of the protein.

(63) Pelton, J. G.; Torchia, D. A.; Meadow, N. D.; Roseman, S. *Protein Sci.* **1993**, *2*, 543–558.
(64) O'Halloran, T. V.; Culotta, V. C. *J. Biol. Chem.* **2000**, *275*, 25057–25060.
(65) Lin, S. J.; Pufahl, R. A.; Dancis, A.; O'Halloran, T. V.; Culotta, V. C. *J. Biol. Chem.* **1997**, *272*, 9215–9220.
(66) Schmidt, P. J.; Rae, T. D.; Pufahl, R. A.; Hamma, T.; Strain, J.; O'Halloran, T. V.; Culotta, V. C. *J. Biol. Chem.* **1999**, *274*, 23719–23725.
(67) Lamb, A. L.; Wernimont, A. K.; Pufahl, R. A.; Culotta, V. C.; O'Halloran, T. V.; Rosenzweig, A. C. *Nat. Struct. Biol.* **1999**, *6*, 724–729.

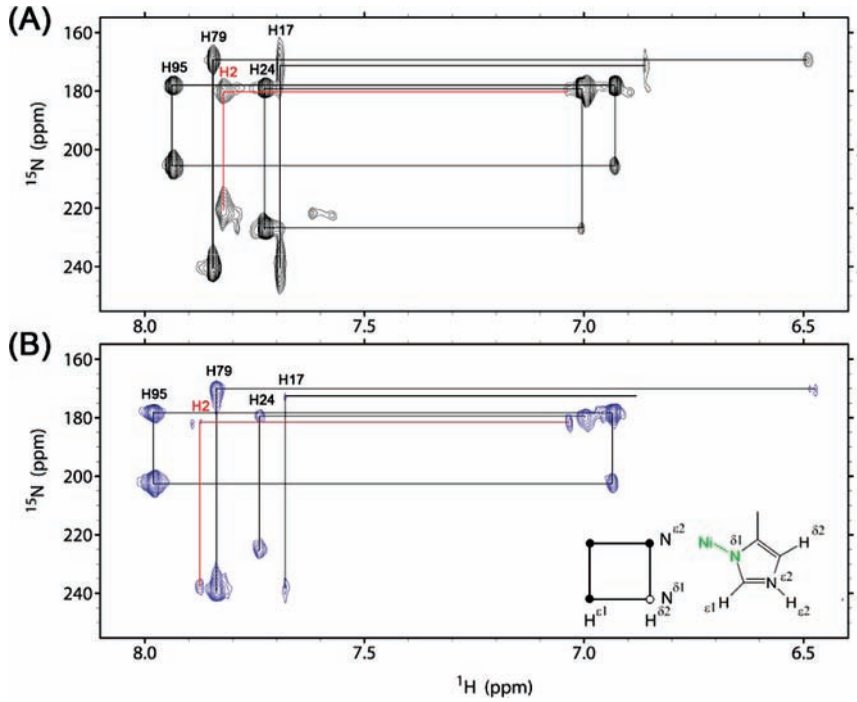

Figure 9. Two-dimensional $^{1}H-^{15}N$ HMQC spectra of histidine side chains of Ni-free, Zn-HypA (A) and Ni-bound, Zn-HypA (B). Note the significant downfield shift of His2 upon Ni^{2+} binding. Combined with the signal pattern, it is clear that nickel ion coordinated to the $N^{\delta 1}$ atom of His2.

ions to the apo-hydrogeanse. In order to understand structure−function relationship of the HypA, the solution structure of Zn-HypA was determined by triple resonance NMR in combination with molecular dynamic calculation. The protein folds into two domains (zinc domain and nickel domain) with a mixed α/β topology, and a distinct metal binding site is located in each domain. Yet, no structural homologues were found for this protein. The structure of *H. pylori* Zn-HypA in this study represents the first for this class of proteins. Two domain structures each with different functions have been found in other metallochaperones such as UreE and the Cu(I) chaperone Atx1. UreE consists of a metal-binding domain at the C-terminus and a peptide-binding domain at the N-terminus.[22,68]

Directly purified recombinant HypA protein obtained in this study was found to contain 1 molar equiv of zinc ion, implying a relatively high zinc-binding affinity toward the HypA. The two CXXC motifs were highly conserved in various microorganisms (Figure 5) and have been proposed to be involved in zinc binding in *E. coli* HypA and HybF proteins.[24,29] In the structures calculated without incorporation of Zn−S cluster restraints, we noticed that the four conserved cysteine residues, Cys74, Cys77, Cys91, and Cys94, are positioned suitably to allow zinc coordination (Figure S4 in Supporting Information). When examining chemical shifts of these cysteines, we found that the C^{β} of the four conserved cysteines are significantly downfield shifts (>4 ppm) compared with those for free cysteines (Cys16 and Cys60). Such downfield shifts have often been observed in many zinc-finger proteins[69] and are characteristic for Zn^{2+} binding. Furthermore, a single peak at 736 ppm from the ^{113}Cd NMR spectrum of ^{113}Cd-reconstituted HypA provided additional evidence that Zn^{2+} coordinates to the four conserved cysteines tetrahedrally. In contrast to a recent study that Zn^{2+} was reported to coordinate to 3S and 1O/N in the absence of Ni^{2+} and was rearranged to 4S upon Ni^{2+} binding,[30] we have found no evidence that binding of Ni^{2+} will alter zinc coordination. First of all, upon Ni^{2+} binding, the ^{113}Cd peak remained unchanged in terms of both the chemical shifts and line widths. Second, Ni^{2+} binding has only caused downfield shifts of $N^{\delta 1}$ of His2, but not other histidines, indicating that zinc coordination remains unchanged upon Ni^{2+} binding. This is reasonable since the two metal-binding sites are ca. 30 Å apart.

Our combined UV−vis (absorption at 420 nm), CD, and NMR data clearly showed that Ni^{2+} is diamagnetic with four nitrogens as donors. Both HSQC and HMQC demonstrated that His2, Glu3, and Asp40 were involved in nickel coordination, and therefore, nickel binding to the protein in a square-planar geometry was proposed, that is, His2 (backbone N and $N^{\delta 1}$), Glu3 (backbone N), Asp40 (backbone N) (Figure 7C). Both His2 and Glu3 are conserved in HypA in microorganisms (Figure 5) and are putative nickel-binding residues. Previously, it was found that mutation of all histidines (His2, His17, His24, His79, and His95) in *Hp*HypA did not affect nickel binding except His2, suggesting that His2 is essential for nickel binding.[23] Similar feature was also observed in *E. coli* HybF. Replacement of Glu3 by a leucine (Leu) was found to disrupt the activity of hydrogenase but not Gln, indicating the amide of Glu plays a critical role in metal binding.[29] The hydrophobic side chain of Leu may affect metal binding to the backbone amide, whereas Gln will not since it has a similar side chain as Glu in view of size and polarity. His2 and Glu3 are located at the beginning of helix 1, whereas Asp40 is at the beginning of helix 2. Movement of the helices may allow those residues to position suitably for metal binding and reversibly to facilitate metal release. Conformational changes of the protein accompanied by nickel binding were observed indeed, and those perturbed residues by Ni^{2+} were mapped in HypA structure (Figure 8).

(68) Remaut, H.; Safarov, N.; Ciurli, S.; Van Beeumen, J. *J. Biol. Chem.* **2001**, *276*, 49365–49370.
(69) Kornhaber, G. J.; Snyder, D.; Moseley, H. N. B.; Montelione, G. T. *J. Biomol. NMR* **2006**, *34*, 259–269.

Square-planar nickel-binding site has been found in many proteins, such as the N-terminus of human serum albumin[70] and NikR. However, a recent report proposed a six-coordinated Ni site with N/O as ligand donors based on XAS data.[30] When we carefully examined the HypA protein structure, we found that those conserved glutamates and aspartic acids in addition to histidines, which were proposed to be potential nickel-binding residues previously, were quite far away from the N-terminus of the protein (Figure S7 in Supporting Information). Such discrepancy may be due to the low affinity of nickel to the protein resulting in partial of the metal dissociation from the protein and exhibiting as a six-coordinated nickel in free solution.

HypA exhibits two distinct metal binding sites located at each domain. Zinc may play a structural role to mediate protein−protein interactions required for a complex formation as reported in other proteins.[71] For example, tetrathiolate zinc site was found to mediate the interaction between ZPR1 with EGFR[72] and *E. coli* heat-shock protein Dnaj with unfolded proteins.[73] Our initial data demonstrated that Zn^{2+} enhances the formation of a HypA·HypB complex (unpublished data). Further investigations of the role of Zn^{2+} in the complexation of HypA with HypB and in Ni^{2+} delivery are warranted.

Many metalloproteins coordinated to their cargo metals with low coordination number, such as Cu(I) in Atx1[74] and As(III)/Sb(III) in ArsA.[75] Low coordination number of Ni^{2+} in HypA may allow metals to be readily transferred to its downstream receptors (e.g., HypB).[76,77] Similar behavior was found for Ni^{2+} in this study with 4N coordinated to Ni^{2+}, suggesting that it may be a common feature for metal coordination in chaperone(s), that is, adopting a low coordination to increase the accessibility of bound metals and subsequently facilitate metal trafficking in vivo. The conformational changes of the protein induced by nickel may mediate the interactions between HypA and HypB. The interaction of HypA and HypB at the molecular level is under investigation in this laboratory.

In summary, we have determined the solution structure of *H. pylori* HypA and characterized its binding properties to both Zn^{2+} and Ni^{2+}. The protein exhibits a unique two-domain architecture with a distinct metal binding site in each domain. Zinc coordinates with four conserved cysteines in the loop region tetrahedrally, and strikingly, nickel binds four nitrogens from backbone amides of residues His2, Glu3, Asp40, and the side chain of His2 in a square-planar geometry. We anticipate that our structure will provide important new insight into nickel trafficking and subsequently the cell biology of nickel.

Acknowledgment. We thank Research Grants Council of Hong Kong (HKU7512/05M, HKU7042/07P, HKU7038/08P), RGC Collaborative Research Fund (HKU1/07C and HKU2/06C), the UGC of Hong Kong SAR of China under the scheme of the Area of Excellence, and the University of Hong Kong for their support. We are grateful to Prof. John H. Viles (QMW, London) and Prof. Sunney Chan (Caltech) for helpful discussion and comments.

Supporting Information Available: Experimental details including molecular biology material list, SDS-PAGE for purified HypA protein, gel filtration analysis of Zn-HypA protein, HypA structure with all potential nickel ligands highlighted, procedure for the apo-form HypA preparation, and complete refs 20 and 21. This material is available free of charge via the Internet at http://pubs.acs.org.

JA900543Y

(70) Laussac, J. P.; Sarkar, B. *Biochemistry* **1984**, *23*, 2832–2838.
(71) Mackay, J. P.; Crossley, M. *Trends Biochem. Sci.* **1998**, *23*, 1–4.
(72) Galcheva-Gargova, Z.; Konstantinov, K. N.; Wu, I. H.; Klier, F. G.; Barrett, T.; Davis, R. J. *Science* **1996**, *272*, 1797–1802.
(73) Szabo, A.; Korszun, R.; Hartl, F. U.; Flanagan, J. *EMBO J.* **1996**, *15*, 408–417.
(74) Portnoy, M. E.; Rosenzweig, A. C.; Rae, T.; Huffman, D. L.; O'Halloran, T. V.; Culotta, V. C. *J. Biol. Chem.* **1999**, *274*, 15041–15045.
(75) Zhou, T. Q.; Radaev, S.; Rosen, B. P.; Gatti, D. L. *EMBO J.* **2000**, *19*, 4838–4845.
(76) Finney, L. A.; O'Halloran, T. V. *Science* **2003**, *300*, 931–936.
(77) Davis, A. V.; O'Halloran, T. V. *Nat. Chem. Biol.* **2008**, *4*, 148–151.
(78) Greenfield, N. J. *Nat. Protoc.* **2006**, *1*, 2876–2890.